Nanoscale

PAPER

View Article Online
View Journal | View Issue

Cite this: *Nanoscale*, 2018, **10**, 1207

Intrinsic rippling enhances static non-reciprocity in a graphene metamaterial†

Duc Tam Ho, [a] Harold S. Park[b] and Sung Youb Kim *[a]

Received 14th October 2017,
Accepted 8th December 2017

DOI: 10.1039/c7nr07651g

rsc.li/nanoscale

In mechanical systems, Maxwell–Betti reciprocity means that the displacement at point B in response to a force at point A is the same as the displacement at point A in response to the same force applied at point B. Because the notion of reciprocity is general, fundamental, and is operant for other physical systems like electromagnetics, acoustics, and optics, there is significant interest in understanding systems that are not reciprocal, or exhibit non-reciprocity. However, most studies on non-reciprocity have occurred in bulk-scale structures for dynamic problems involving time reversal symmetry. As a result, little is known about the mechanisms governing static non-reciprocal responses, particularly in atomically-thin two-dimensional materials like graphene. Here, we use classical atomistic simulations to demonstrate that out-of-plane ripples, which are intrinsic to graphene, enable significant, multiple orders of magnitude enhancements in the statically non-reciprocal response of graphene metamaterials. Specifically, we find that a striking interplay between the ripples and the stress fields that are induced in the metamaterials due to their geometry impacts the displacements that are transmitted by the metamaterial, thus leading to a significantly enhanced static non-reciprocal response. This study thus demonstrates the potential of two-dimensional mechanical metamaterials for symmetry-breaking applications.

Introduction

Reciprocity is a fundamental physical principle that has significant implications for a range of scientific disciplines. Essentially, reciprocity implies that the response of a structure at point B to an excitation at point A will be the same as the response of the structure at point A to an excitation at point B, and that this is independent of variations in geometry or material properties. In structural mechanics, this is formalized through the Maxwell–Betti reciprocity theorem, which states that the displacement of point B due to a force at point A is the same as the displacement of point A due to a force at point B. Mathematically, this is written as

$$F_A u_{B\to A} = F_B u_{A\to B}$$

where F_A is the force applied to point A, and $u_{A\to B}$ is the displacement of point B induced by F_A. Because reciprocity is a general and fundamental physical principle with applications across the scientific spectrum in electromagnetism, optics, acoustics and mechanics, there has been significant recent interest in systems that break reciprocity, or are non-reciprocal.[1–4] In mechanical systems, this has predominately been for dynamic problems involving wave propagation to break time-reversal symmetry.[1–9] Breaking time-reversal symmetry would enable novel applications and functionality by controlling the direction of wave propagation, enabling filtering and isolation, preventing information backscattering like echoing, and acoustic amplification.

In contrast, while many mechanical systems operate within the static regime, there have been significantly fewer studies on static non-reciprocity in mechanical systems. Recently, Coulais and co-workers performed a seminal study investigating static non-reciprocity in mechanical structures.[10] By combining large nonlinearities and geometric asymmetry, they were able to induce non-reciprocal deformations in both a fishbone structure as well as a mechanical metamaterial. The observation of non-reciprocity in a metamaterial is important both due to the increasing interest in mechanical metamaterials, as well as the recent reports of novel functionality and properties which they have been found to exhibit.[11–16]

However, nearly all reported studies on non-reciprocal behavior have been for bulk-scale structures, and so with the exception of one report we are aware of onsignal isolation in multilayer graphene nanoribbons,[5] there is little understanding of the mechanisms governing static non-reciprocity at the nanoscale, and specifically for two-dimensional (2D) mechanical metamaterials. In this work, we investigate the potential of graphene, the canonical 2D material, as a statically non-

[a]*Department of Mechanical Engineering, Ulsan National Institute of Science and Technology, Ulsan 44919, South Korea. E-mail: sykim@unist.ac.kr*
[b]*Department of Mechanical Engineering, Boston University, Boston, MA 02215, USA*
†Electronic supplementary information (ESI) available. See DOI: 10.1039/c7nr07651g

reciprocal mechanical metamaterial. Graphene is in many ways an ideal material for studies on non-reciprocity, due to its ability to undergo large, geometric shape changes resulting from its relatively low bending modulus.[17] We demonstrate that the presence of out-of-plane ripples, whether they emerge from long wavelength fluctuations,[18] from edge stresses,[19,20] or from external strain,[21] leads to multiple orders of magnitude enhancement in the static non-reciprocity as compared to structures in which out-of-plane deformation does not occur. Our studies thus point to the potential of 2D materials as the basic building blocks of non-reciprocal nanoscale metamaterials.

Results and discussion

Non-reciprocity of the planar graphene metamaterial

The monolayer graphene metamaterial, we consider in this work, is illustrated in Fig. 1. This graphene metamaterial is the 2D monolayer analog of the mechanical metamaterial structure considered by Coulais and co-workers in Fig. 3 of their paper.[10] The metamaterial consists of diamond and square shaped monolayers of graphene that are connected *via* thin ligaments, and the structural asymmetry is governed by the angle θ. Molecular statics (MS) simulations with different techniques were used to investigate the non-reciprocity. In the first MS simulation approach, no perturbation along the out-of-plane direction is added, and we call this approach the 2D MS simulation. In the second MS simulation approach, the results of which are discussed in detail later, small random perturbations, which are used to induce out-of-plane rippling, are added to the out-of-plane (z)-displacements before any external loading is applied. We call this approach the perturbed MS simulation. These simulations will enable us to quantify the effect of intrinsic, out-of-plane ripples on the static non-reciprocity as compared to the planar 2D MS simulations. Details of the geometry of the graphene metamaterials and atomistic simulation methods can be seen in the Simulation methods section.

We first discuss the 2D MS results, to highlight the static non-reciprocity of graphene when out-of-plane distortions do not occur, as in the bulk mechanical metamaterial studied by Coulais *et al.*[10] Similar to the work of Coulais *et al.*, we define the non-reciprocity parameter to be $\Delta u = u_{0,R} + u_{3,L}$, where $u_{0,R}$ is the displacement of node A_0 due to the applied force at the right end in Fig. 1, while $u_{3,L}$ is the displacement at node A_3 due to the applied force at the left end. Fig. S1 in the ESI† illustrates the structural response of the graphene metamaterial to an external force 1.4 eV Å^{-1} applied at the right end (node A_3 in Fig. 1), and also at the left end (node A_0 in Fig. 1). It is clear from Fig. S1† that significantly larger deformation is observed when the force is applied at the right end than at the left end of the metamaterial, similar to the observation by Coulais *et al.*[10] The displacement field for the graphene metamaterial shown in Fig. S1† exhibits a large value at the right end, but with a large, nonlinear decay with the distance away from the right end. Thus, for $\theta > 0$, when we pull the structure from the right end, the displacement is large at the right end ($u_{3,R}$ is large) and it decreases significantly moving towards the left end. In contrast, the displacement at the left end node A_0 due to the force applied at the right end $u_{0,R}$ is much smaller than $u_{3,R}$. However, $u_{0,R}$ is still larger than $u_{3,L}$ and thus a non-reciprocal response of the graphene metamaterial is observed as demonstrated in Fig. 2a.

Fig. 2a quantifies the response of the graphene metamaterial for two different asymmetry angles, $\theta = \pi/32$ and $\theta = \pi/16$. For small forces, the relationship between the displacement and the applied force is quadratic, $\Delta u = \kappa F^2$. Fig. 2a demonstrates that the structure with $\theta = \pi/32$ is more asymmetric than the one with $\theta = \pi/16$, and also exhibits a larger displacement. This is shown more concretely by plotting the susceptibility parameter κ as a function of asymmetry angle in Fig. 2b, where we find, similar to the analysis of Coulais *et al.*, a divergence in the susceptibility parameter as the asymmetry angle $\theta \to 0$.

These 2D MS simulations serve to demonstrate that, like the bulk metamaterials studied by Coulais *et al.*,[10] 2D graphene metamaterials with the same geometry and with the same in-plane deformations in response to the applied forces also exhibit static non-reciprocity, while also illustrating the potential of highly non-reciprocal graphene metamaterials for small asymmetry angles as illustrated in Fig. 2b. However, the key question we wish to address in this work is this: what effects do physics that are unique or intrinsic to 2D materials, and that do not exist in bulk materials have on the static non-reciprocity of graphene metamaterials? We examine this next using MS simulations with small perturbations in the out-of-plane direction.

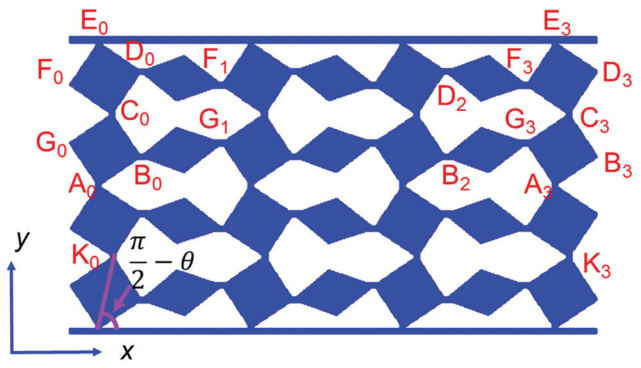

Fig. 1 Schematic of the graphene metamaterial, with different nodes labelled along with the asymmetry angle θ.

Non-reciprocity of the rippled graphene metamaterial

We now examine the effects that out-of-plane ripples, which are intrinsic to graphene,[18] have on the static non-reciprocity. To do so, we performed perturbed MS simulations, where small random displacements in the out-of-plane (z)-direction were applied to all atoms to mimic the effects of intrinsic rippling. Because of our interest in static, and not dynamic non-reciprocity, the small out-of-plane perturbations enabled us to

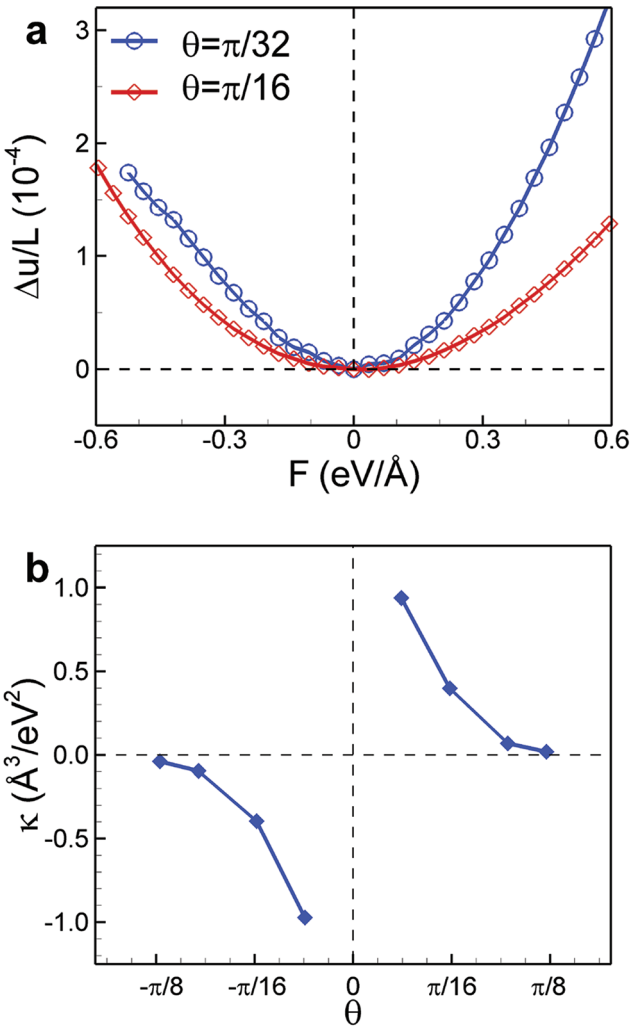

Fig. 2 Non-reciprocity in the planar graphene metamaterials obtained by 2D MS simulation. (a) The change of the non-reciprocity parameter $\Delta u/L$ with the applied force for different asymmetry angles where L is the length of the graphene structure along the horizontal direction. (b) Non-reciprocity susceptibility parameter $\kappa = \Delta u/F^2$ *versus* the asymmetry angle.

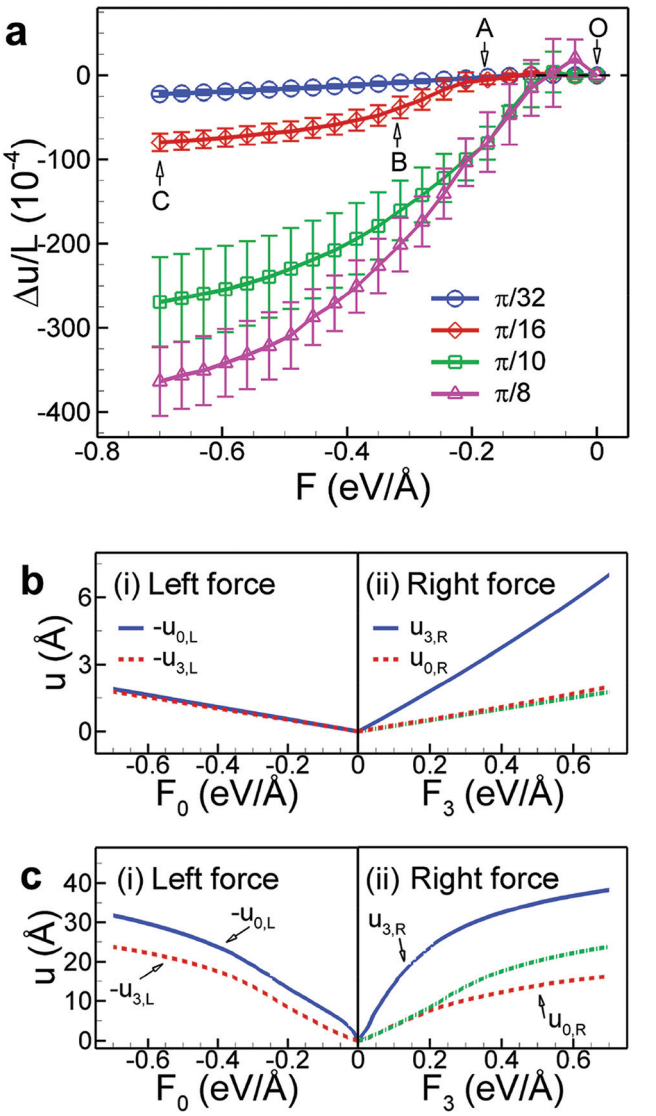

Fig. 3 Non-reciprocity in the graphene metamaterials depicted in Fig. 1 obtained by perturbed MS simulations. (a) The change of the non-reciprocity parameter of the graphene metamaterial with the applied force. As discussed in the text, A denotes the low force regime (forces smaller than 0.18 eV Å^{-1}), B denotes forces in the intermediate regime (0.18 eV Å^{-1} < F < 0.32 eV Å^{-1}), and C denotes the high force regime (larger than about 0.32 eV Å^{-1}). The standard deviation was used to qualify the variation of the results. 2D MS simulation displacements at (b-i) nodes A_0 and A_3 due to the forces applied at the left end (nodes A_0); (b-ii) nodes A_0 and A_3 due to the forces applied at the right end (node A_3). Perturbed MS simulations displacements at (c-i) nodes A_0 and A_3 due to the forces applied at the left end (node A_0); (c-ii) nodes A_0 and A_3 due to the forces applied at the right end (node A_3). The green dashed and dotted lines in (b-ii) and (c-ii) are the mirror images of the red dash lines in (b-i) and (c-i), respectively; the line of refection is the vertical center line. For b–c, the asymmetry angle of $\theta = \pi/16$ was considered. Note the significantly enhanced displacements in (c) with rippling as compared to (b) without rippling.

generate out-of-plane ripples without the need for thermal fluctuations, which are a dynamic property. This further enabled us to isolate the effects of ripples on the static non-reciprocity *via* quasi-static MS simulations, without needing to utilize high strain-rate, dynamic molecular dynamics (MD) simulations.

The rippling is stochastic; 4 different perturbed MS simulations with different initial random perturbations in the z-direction were conducted, where we note that the energy of the equilibrium configuration of the graphene metamaterials with out-of-plane ripples is smaller than that of the flat graphene metamaterial without rippling, indicating that the rippled configuration is more energetically favorable than the flat configuration. Fig. S2 in the ESI† demonstrates that a different rippling pattern will be observed throughout the metamaterial depending on the initial random perturbation. This is because different parts of the metamaterial can ripple in the positive or negative out-of-plane directions depending on the sign of the perturbation. However, we will demonstrate

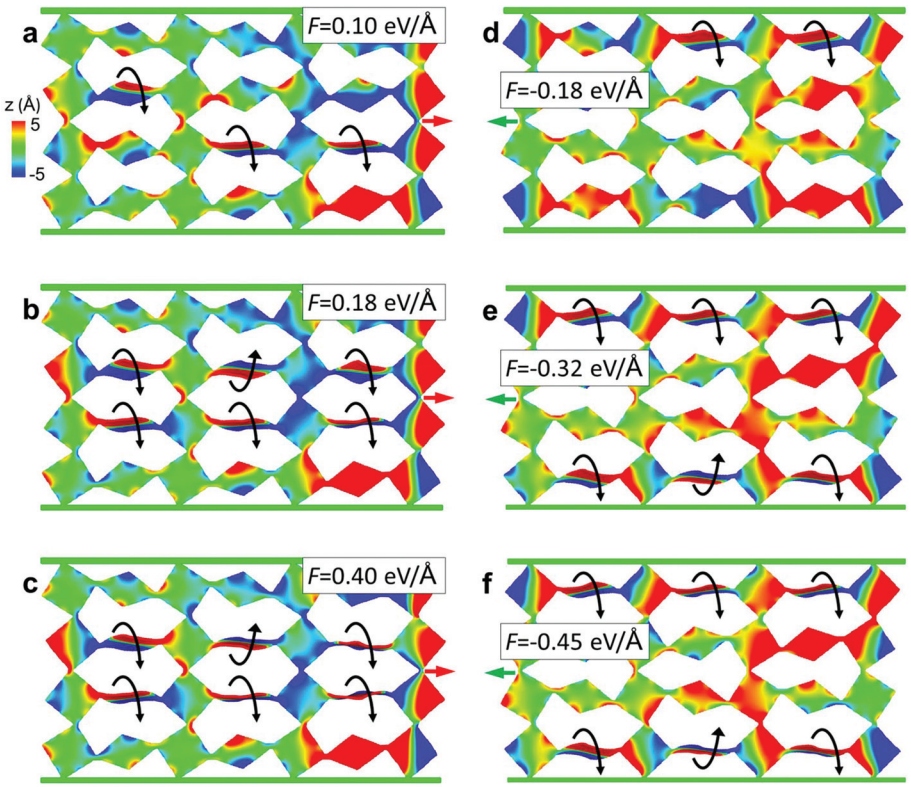

Fig. 4 The configurations of the graphene metamaterial with the asymmetry angle $\theta = \frac{\pi}{16}$ under different applied forces at the right end (a–c) and at the left end (d–f).

below that the stochastic nature of the rippling that is observed in the equilibrated structures in Fig. S2† before forces are applied does not impact the results that we report.

Fig. 3a shows the non-reciprocity parameter obtained by the perturbed MS simulations with out-of-plane rippling. In comparison with Fig. 2a, where out-of-plane rippling was not considered, two important factors have changed. First, the non-reciprocity parameter is larger by two orders of magnitude when rippling is accounted for. Second, the sign of the non-reciprocity parameter when rippling is accounted for is negative, which is different from the flat graphene metamaterial in Fig. 2a.

Fig. 3 also presents the changes of the displacements at nodes A_0 and A_3 of the graphene metamaterial depicted in Fig. 1 under loading obtained by the 2D MS simulations (Fig. 3b) as well as perturbed MS simulations (Fig. 3c). The perturbed MS displacements shown in Fig. 3c are different from the 2D MS displacements in Fig. 3b in two aspects. First, the displacements obtained by the perturbed MS simulations are much larger than those of the 2D MS simulations; we will mechanistically demonstrate later that this is due to the out-of-plane rippling. Second, the displacement is a nonlinear function of loading in the perturbed MS simulations as shown in Fig. 3c, which is different from the linear force-displacement relationship seen in the 2D MS simulations in Fig. 3b. The linearity of the displacement curves in Fig. 3b indicates that the stiffness of the 2D MS structures does not change with the applied load. On the other hand, all curves of the perturbed MS results in Fig. 3c are concave, *i.e.* the displacements increase with applied force but the incremental change decreases. This indicates that the stiffness of the rippled graphene metamaterial structures increases as the applied load increases.

Although the displacements in the perturbed MS simulations are larger than those of the 2D MS results, the degree of enhancement of the displacements (in the comparison with the 2D MS simulation) when the metamaterial is pulled at the right end is smaller than when the metamaterial is pulled from the left end. For example, as can be seen in Fig. 3(b and c), for the applied force of magnitude 0.35 eV $Å^{-1}$, $|u_{3,L}|$ obtained by the perturbed MS simulation in Fig. 3(c-i) is about 15 times larger than the corresponding 2D MS displacement in Fig. 3(b-i) whereas $|u_{0,R}|$ obtained by the perturbed MS simulation is only about 10 times larger than the corresponding 2D MS displacement. Consequently, $|u_{0,R}|$ is smaller than $|u_{3,L}|$ leading to the negative non-reciprocity parameter as shown in Fig. 3a.

Fig. 4(a–c) present the configurations of the rippled graphene metamaterial with the angle $\theta = \frac{\pi}{16}$ when it is pulled from the right end with different force magnitudes; the out-of-plane (z)-displacement magnitudes are shown. When the applied force increases as shown in Fig. 4(a–c), a notable dis-

placement mode is observed (see ESI movies†). Specifically, for forces smaller than 0.18 eV Å^{-1}, the diamonds in the two center-rows rotate out of the *xy*-plane about the *x*-axis as shown in Fig. 4a. After the force reaches 0.18 eV Å^{-1}, all diamond elements in the two middle rows have rotated out of the *xy*-plane, as shown in Fig. 4b. As the force increases beyond 0.18 eV Å^{-1}, the *y*-coordinates of the ligaments connecting the diamond elements to their square neighbors begin to align, with the alignment due to the applied tensile force essentially finishing when the force reaches 0.4 eV Å^{-1} as shown in Fig. 4c.

We observed a strong correlation between the rotation of the diamonds and the displacements $u_{0,R}$ and $u_{3,R}$. Specifically, below a critical value of the applied force, the displacements $|u_{0,R}|$ and $|u_{3,R}|$ increase linearly as the applied force increases, as shown in Fig. 3(c-ii). However, those displacements increase non-linearly when the applied forces exceeds about 0.18 eV Å^{-1}, which is when all diamonds in the center two rows have rotated out of the *xy*-plane. The stiffening of the rippled metamaterials shown in Fig. 3(c-ii) occurs when the applied force exceeds 0.18 eV Å^{-1} because the displacement of the metamaterial shifts from the combination of in-plane stretching of the connecting ligaments and out-of-plane rotation of the center-row diamonds to primarily high energy in-plane stretching of all connecting ligaments.

The rotational displacement of the diamond elements is also observed in the rippled graphene metamaterial when pulled from the left end (see ESI movies†), though there are differences from the case of pulling from the right end that was just discussed. First, Fig. 4(d–f) show that it is the diamonds in the two boundary rows rather than the two center rows that rotate out of the *xy*-plane about the *x*-axis as the force increases. Second, the magnitude of the critical force at which all boundary-row diamonds have rotated out of the *xy*-plane is 0.32 eV Å^{-1}, which is larger than the critical force of 0.18 eV Å^{-1} when the rippled metamaterial is pulled from the right end. After the out-of-plane rotation of the diamond elements is completed, the metamaterial is again forced to deform *via* high energy stretching of the elements and ligaments, which increases the stiffness of the structure when the applied force exceeds the critical force. That explains why both displacements $|u_{0,L}|$ and $|u_{3,L}|$ in Fig. 3(c-i) increase linearly with force when the applied force is smaller than 0.32 eV Å^{-1}, and why both displacements increase non-linearly when the left end pulling force exceeds 0.32 eV Å^{-1}.

The rotational modes are what enable the significant increases in the magnitude of the non-reciprocal behavior for the graphene metamaterial with out-of-plane rippling. Fig. 3a shows that the non-reciprocity is two orders of magnitude larger than that for the graphene metamaterial that is constrained to remain planar in Fig. 2a, where the 2D MS simulations of the planar graphene metamaterial showed similar static non-reciprocity to the macroscale experiments of Coulais *et al.*[10] Specifically, Fig. 3a demonstrates that the graphene metamaterials with out-of-plane rippling exhibit three distinct regimes of static non-reciprocity.

The first regime is for forces smaller than 0.18 eV Å^{-1}, which is the range OA in Fig. 3a. Here, there is a smaller increase in non-reciprocity, though it is important to note that the value of the non-reciprocity parameter reaches nearly 100, which is still two orders of magnitude larger than the value of non-reciprocity of ~1 for the 2D planar graphene metamaterial shown in Fig. 2a. This coincides, as shown in Fig. 4(a and b), with the emergence of the diamond rotation mechanism. For this force range, both displacements $|u_{0,R}|$ and $|u_{3,L}|$ increase linearly with the applied force as shown in Fig. 3b, so the rate of increase in the non-reciprocity parameter is smaller than that for the next regime.

The second regime is when the applied force is in the intermediate range (0.18 eV/Å < F < 0.32 eV Å^{-1}, the range AB in Fig. 3a). Here, the displacement $|u_{3,L}|$ continues to increase with the applied force since the rotational mode in the case of pulling from the left continues to evolve as shown in Fig. 4(d and e), whereas the displacement $|u_{0,R}|$ has a smaller increase because the rotational mechanism in the case of pulling from the right has completed, as shown in Fig. 4b. Therefore, the largest increases in non-reciprocity are observed in Fig. 3a for this force range.

The final regime is for forces larger than about 0.32 eV Å^{-1}, which is the range BC as shown in Fig. 3a. As shown in Fig. 4f, all metamaterial elements have rotated and aligned when pulling from the left, and thus in-plane stretching dominates and $|u_{3,L}|$ begins to increase more slowly, as shown in Fig. 3a, leading to a decrease in the rate of increase in the non-reciprocity.

The final question we address is to explain not only why the rotational mechanism occurs, but also why the top and bottom rows exhibit the rotational mechanism when the metamaterial is pulled from the left in Fig. 4(d–f), whereas the middle two rows rotate when the metamaterial is pulled from the right in Fig. 4(a–c). The mechanism for pulling to the right is shown in Fig. 5(a–c) and S3.† When the metamaterial is pulled to the right, a significant compressive stress is generated in the two center squares of the last column, as shown in Fig. S3(a).† This is because the two squares in rows 2 and 3 act as two bars connected at a hinge, where due to the angle of connection, the applied force to the right generates compression in both bars as shown in Fig. S3(b).† As shown in Fig. S3(a),† the compressive stress first generates an enhancement in the rippling amplitude, with part of the square element rippling in the positive *z*-direction, and the other part rippling down in the negative *z*-direction. The square element with nodes at $A_3B_3C_3G_3$ then rotates counterclockwise, which leads to a clockwise rotation of the diamond with nodes at B_2 and G_3 as shown in Fig. 5a. Furthermore, as shown in Fig. 5b and c, a portion of the ligament connecting square $A_3B_3C_3G_3$ and the diamond element is under compression, which causes out-of-plane buckling of that ligament portion. Because one portion of the ligament is under compression, leading to out-of-plane buckling, while the other part is in tension, rotation of the diamond element out of the *xy*-plane about the *x*-axis is observed with increasing force. The other connecting diamond

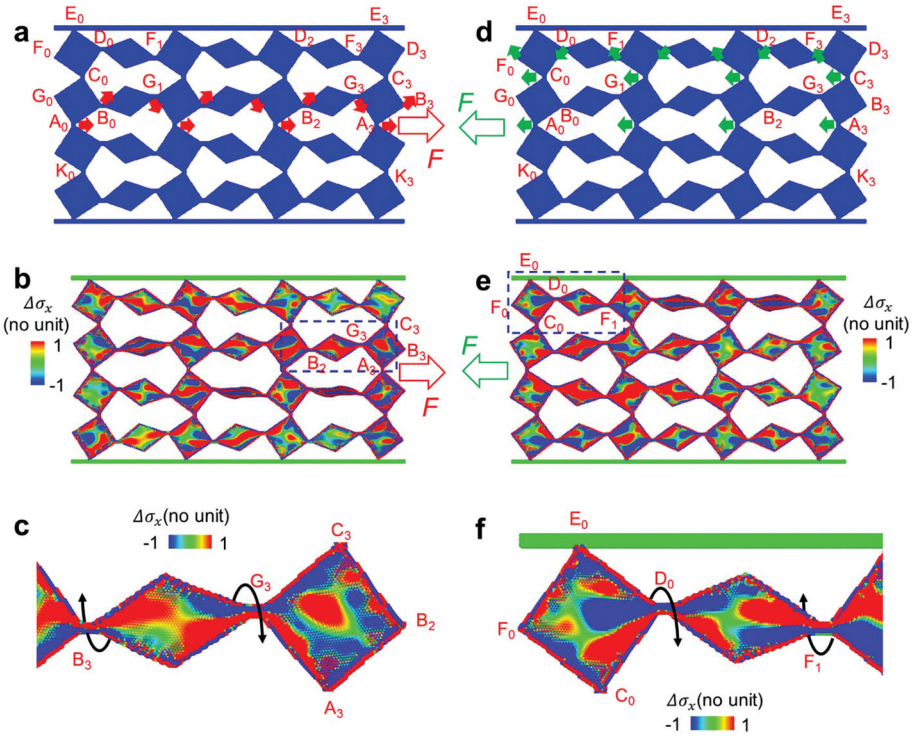

Fig. 5 Displacement and stress fields resulting from the applied force at the right end (a–c) and from the applied force at the left end (d–f) when rippling is considered. (a, d) Displacements, and (b–c, e–f) stress fields. Only displacements at some nodes are shown. For (b–c), the force F = 0.11 eV Å^{-1} is applied, and for (e–f), the force F = −0.175 eV Å^{-1} is applied. The rotation of center row diamonds (for the case of applying force from the right) and boundary diamonds (for the case of applying force from the left) out of the xy-plane about the x-direction can be observed due to the buckling of the ligaments which is due to the compressive axial stress in these ligaments. The asymmetry angle $\theta = \pi/16$ was considered.

elements in the center two rows exhibit a similar deformation transition as the load is transferred to them from enhanced out-of-plane rippling to rotation of the element about the out of plane (z)-axis as force increases.

However, when force is applied to the left end, the rotational mechanism occurs in different rows of the metamaterial, as shown in Fig. 5d. This is because a tensile stress is generated in the square elements as shown in Fig. S4(a)† due to the angle of connection shown in Fig. S4(b).† The tensile stress acts to flatten out the ripples as shown in Fig. S4(a),† and thus a rotation of the elements in the center two rows leading to rotation of the connecting diamond elements is not observed. However, the response of the boundary row elements is different. Because the center rows move to the left when pulled at A_0, node C_0 shown in Fig. 1 is also pulled to the left as shown in Fig. 5d. This causes clockwise in-plane rotation of the top left square element $C_0F_0E_0D_0$. This rotation results in both compressive and tensile stresses in the ligament at node D_0 (Fig. 5e and f). As the force increases, the compressive stress becomes sufficient to cause out-of-plane buckling of a portion of the connecting ligament, whereas the remainder of the ligament is under tension. This, as with the pulling to the right case, leads to rotation of the diamond element out of the xy-plane. As the force is increased, other diamond elements in the top and bottom rows exhibit the out-of-plane rotational mechanism; the square elements in those rows do not exhibit the rotational mechanism as they are more constrained by having three connected nodes, including one node fixed to the boundary rows.

We believe that the specific metamaterial structure considered here, for monolayer graphene, and at the bulk by Coulais *et al.*,[10] should lead to non-reciprocal behavior across length scales ranging from the atomic scale to the macro-scale. However, the magnitude of the non-reciprocity will depend on the specific material that is chosen. As an example of such scaling across length scales, researchers have shown that specific kirigami metamaterials exhibit similar size-independent behavior regardless of whether they are at the nanoscale[22,23] for a crystalline solid such as graphene or MoS_2, or at the macroscale for a soft kirigami actuator.[24]

Finally, we note that strain-rate and temperature are likely to impact the non-reciprocity. For example, strain-rate strongly effects on the buckling of 2D structures *i.e.*, the critical load for buckling increases significantly as the strain-rate increases.[25] Therefore, we may expect that high strain rates may delay the out-of-plane buckling and low energy rotational deformation in the graphene metamaterial, which would decrease the effect of the rippling and reduce the magnitude of the non-reciprocity.

At high temperature, there may be a competition between elastic softening of the ligaments favoring an increase in non-reciprocity with the decrease in structural stability, particularly

for the monolayer 2D materials as considered here. Overall, the effects of the strain rate and temperature on the non-reciprocity of the 2D metamaterials are important ones, which we are currently investigating.

Conclusion

We have used MS simulations to demonstrate that out-of-plane rippling, which is intrinsic to graphene, results in enhancements of the static non-reciprocity by two orders of magnitude as compared to graphene metamaterials that do not exhibit an out-of-plane deformation. In particular, the intrinsic rippling enables a unique, low energy rotational deformation in the graphene metamaterial. The asymmetry of the applied forces at the left and right ends that are needed to complete the rotational mechanism leads to a window of applied forces in which the static non-reciprocity increases significantly. The present results not only demonstrate the potential enhancements in non-reciprocity that can be enabled through out-of-plane deformations in atomically-thin 2D metamaterials, but also demonstrate the possibility of achieving sign-tunable non-reciprocal behavior.

Simulation methods

The monolayer graphene metamaterials consist of about 80 000 carbon atoms, which were modeled using the second generation Rebo (REBO-II) potential, which has been shown to well-represent the large-strain mechanical behavior and properties of graphene.[26] We assigned the zigzag and armchair directions as the *x*- and *y*-directions, respectively. The dimensions of the graphene metamaterial in the *x*- and *y*-directions are 90 nm and 50 nm, respectively. The square edge length is about 9 nm, and the diagonal lengths of the diamonds are about 14 nm and 7 nm. The size of the ligaments which connect the vertices of the polygons is about 1 nm. We confirmed that there is no defect-mediated deformation and fracture in the ligaments in the range force we applied (Fig. S5 in ESI†). No periodic boundary conditions were applied in any direction. The top and bottom edges of the metamaterial were held fixed (see solid horizontal lines in Fig. 1), while forces were applied to either node A_0 or node A_3 as shown in Fig. 1, in order to calculate the degree of static structural non-reciprocity. Molecular statics (MS) simulations were used to investigate the non-reciprocity, using the publicly-available simulation code LAMMPS.[27] The open visualization tool OVITO was used for all visualizations.[28]

As mentioned previously, we employed 2D MS simulations as well as perturbed MS simulations. The enhancements in non-reciprocity due to out-of-plane distortions were found by performing MS simulations with an initial out-of-plane perturbation. Specifically, the out-of-plane distortions, or rippling, are induced by adding small random perturbations to the out of plane (z)-displacements before any external loading is applied. The MS simulations correspond to a zero temperature (0 K) static simulation in which the equilibrium positions of the atoms in response to applied loading are found through energy minimization, and correspond to a situation in which thermal energy is absent from the system. The conjugate gradient method was used for all minimizations where a set of atomic positions in response to a specific external force is deemed to be convergent if the energy change between successive iterations divided by the energy magnitude is less than 10^{-14}. In all MS simulations, before applying force, each structure was fully relaxed to attain the equilibrium state, after which forces were applied in increments of 0.007 eV $Å^{-1}$.

Conflicts of interest

There are no conflicts to declare.

Acknowledgements

We gratefully acknowledge the support from the ICT R&D Program (No R0190-15-2012) of Institute for Information communications Technology Promotion (IITP) and from the Mid-Career Researcher Support Program (Grant No. 2014R1A2A2A09052374) of the National Research Foundation (NRF), which are funded by the MSIP of Korea. We also acknowledge with gratitude the PLSI supercomputing resources of the KISTI and the UNIST Supercomputing Center. HSP acknowledges the support of the Mechanical Engineering department at Boston University.

References

1 R. Fleury, D. L. Sounas, C. F. Sieck, A. Haberman and M. R. Alu, *Science*, 2014, **343**, 516–519.
2 H. Nassar, X. C. Xu, A. N. Norris and G. L. Huang, *J. Mech. Phys. Solids*, 2017, **101**, 10–29.
3 N. Swinteck, S. Matsuo, K. Runge, J. O. Vasseur, P. Lucas and P. A. Deymier, *J. Appl. Phys.*, 2015, **118**, 063103.
4 M. B. Zanjani, A. R. Davoyan, A. M. Mahmoud, N. Engheta and J. R. Lukes, *Appl. Phys. Lett.*, 2014, **104**, 081905.
5 M. B. Zanjani, A. R. Davoyan, N. Engheta and J. R. Lukes, *Sci. Rep.*, 2015, **5**, 09926.
6 S. A. Cummer, A. Christensen and J. Alu, *Nat. Rev. Mater.*, 2016, **1**, 16001.
7 R. Fleury, D. Sounas and A. Alu, *Nat. Commun.*, 2014, **6**, 5905.
8 X. Zhu, H. Ramezani, C. Shi, J. Zhu and X. Zhang, *Phys. Rev. X*, 2014, **4**, 031042.
9 G. Trainiti and M. Ruzzene, *New J. Phys.*, 2016, **18**, 083047.
10 C. Coulais, D. Sounas and A. Alù, *Nature*, 2017, **542**, 461–464.
11 B. Florijn, C. Coulais and M. Van Hecke, *Phys. Rev. Lett.*, 2014, **113**, 175503.
12 R. Lakes, *Science*, 1987, **235**, 1038–1040.
13 A. E. Nicolaou and Z. G. Motter, *Nat. Mater.*, 2012, **11**, 608–613.
14 M. Schenk and S. D. Guest, *Proc. Natl. Acad. Sci. U. S. A.*, 2013, **110**, 3276–3281.

15 J. L. Silverberg, A. A. Evans, L. Mcleod, R. C. Hayward, T. Hull, C. D. Santangelo and I. Cohen, *Science*, 2014, **345**, 647–650.
16 X. Zheng, W. Smith, J. Jackson, B. Moran, H. Cui, D. Chen, J. Ye, N. Fang, N. Rodriguez, T. Weisgraber and C. M. Spadaccini, *Nat. Mater.*, 2016, **15**, 1100–1106.
17 Q. Lu, M. Arroyo and R. Huang, *J. Phys. D: Appl. Phys.*, 2009, **102002**, 5.
18 M. I. Fasolino, A. Los and J. H. Katsnelson, *Nat. Mater.*, 2007, **6**, 858–861.
19 V. B. Shenoy, C. D. Reddy, A. Ramasubramaniam and Y. W. Zhang, *Phys. Rev. Lett.*, 2008, **101**, 245501.
20 H. S. Park and J. W. Jiang, *Nano Lett.*, 2016, **16**, 2657–2662.
21 U. Monteverde, J. Pal, M. A. Migliorato, M. Missous, U. Bangert, R. Zan, R. Kashtiban and D. Powell, *Carbon*, 2015, **91**, 266–274.
22 M. K. Blees, A. W. Barnard, P. A. Rose, S. P. Roberts, K. L. McGill, P. Y. Huang, A. R. Ruyack, J. W. Kevek, B. Kobrin, D. A. Muller and P. L. McEuen, *Nature*, 2015, **524**, 204–207.
23 Z. Qi, D. K. Campbell and H. S. Park, *Phys. Rev. B: Condens. Matter Mater. Phys.*, 2014, **90**, 245437.
24 M. A. Dias, M. P. McCarron, D. Rayneau-Kirkhope, P. Z. Hanakata, D. K. Campbell, H. S. Park and D. P. Holmes, *Soft Matter*, 2017, **13**, 9087–9092.
25 J.-W. Jiang, *Sci. Rep.*, 2015, **5**, srep07814.
26 D. W. Brenner, O. A. Shenderova, J. A. Harrison, S. J. Stuart, B. Ni and S. B. Sinnott, *J. Phys.: Condens. Matter*, 2002, **14**, 783.
27 S. Plimpton, *J. Comput. Phys.*, 1995, **117**, 1–19.
28 A. Stukowski, *Model. Simul. Mater. Sci. Eng.*, 2010, **18**, 015012.